# MRI of *Capn15* knockout mice and analysis of *Capn15* distribution reveal possible roles in brain development and plasticity

Congyao Zha[1]#, Carole A Farah[1]#, Vladimir Fonov[1], David A. Rudko[1,2], and Wayne S Sossin[1]*

[1]*Department of Neurology and Neurosurgery, Montreal Neurological Institute, McGill University, Montreal, Quebec, Canada, H3A 2B4*

[2]*Department of Biomedical Engineering, McGill University, Montreal, Quebec, Canada,*

#Equally contributed

*Corresponding author: Wayne S Sossin; Email: wayne.sossin@mcgill.ca; Phone 1-514-398-1486

Running Title: The role of Calpain 15 in mouse brain

Manuscript Category: Article

**Abstract**

**Purpose:** The non-classical Small Optic Lobe (SOL) family of calpains are intracellular cysteine proteases that are expressed in the nervous system and appear to play an important role in neuronal development in both *Drosophila*, where loss of this calpain leads to the eponymous small optic lobes, and in mouse and human, where loss of this calpain (Capn15) leads to eye anomalies. However, the brain regions where this calpain is expressed and the areas most affected by the loss of this calpain have not been carefully examined.

**Procedures:** We utilize an insert strain where lacZ is expressed under the control of the *Capn15* promoter, together with immunocytochemistry with markers of specific cell types to address where Capn 15 is expressed in the brain. We use small animal MRI comparing WT, *Capn15* knockout and *Capn15* conditional knockout mice to address the brain regions that are affected when Capn 15 is not present, either in early development of the adult.

**Results:** Capn15 is expressed in diverse brain regions, many of them involved in plasticity such as the hippocampus, lateral amygdala and Purkinje neurons. *Capn15* knockout mice have smaller brains, and present specific deficits in the thalamus and hippocampal regions. There are no deficits revealed by MRI in brain regions when *Capn15* is knocked out after development.

**Conclusions:** Areas where Capn15 is expressed in the adult are not good markers for the specific regions where the loss of Capn15 specifically affects brain development. Thus, it is likely that this calpain plays distinct roles in brain development and brain plasticity.

**Keywords:** calpains, hippocampus, brain development, Purkinje neurons, small animal MRI, brain size, SOL,

## Introduction

Calpains are intracellular cysteine proteases that were first discovered in rat brain [1]. There are four conserved families of calpains: Classical, PalB (phosphatase mutants: loss in activity at alkaline pH, but normal or increased activity at acidic pH), Transformer (Tra), and Small Optic Lobe (SOL) with the classical being the best characterized family. All calpain isoforms have a conserved catalytic domain and each calpain family has unique domains: a C-terminal penta-EF hand domain in classical calpains; a C-terminal C2 domain in Tra calpains; an N-terminal MIT domain and an additional C-terminal C2 like domain in PalB calpains, and an N-terminal zinc finger domain that binds polyubiquitin [2] and a C-terminal SOL homology domain in SOL calpains [3-4]. The most ancient family of calpains is PalB, which is expressed in Fungi, followed by SOL expressed in the earliest metazoans, while Tra and Classical calpains diverged from PalB in early pre-bilaterains [4]. Thus, of the four families of calpains present throughout bilaterians, SOL is the most diverged [4].

Calpains play diverse roles in cellular physiology. For instance, degradation of repressors of plasticity by classical calpain, Capn1, in the hippocampus is important for the induction of synaptic plasticity associated with memory [5-7]. Another distinct classical calpain, Capn2, plays an opposite role in limiting plasticity [8-9]. Furthermore, *Capn2* deletion from birth results in embryonic lethality [10] demonstrating multiple distinct roles for this specific calpain. However, while the role of the classical calpains has been well characterized, the role of the other calpain family members in vertebrates is less clear.

SOL calpain was first characterized in the fruit fly *Drosophila* [11-12] where loss of the SOL calpain lead to a 50% reduction in the volume of *Drosophila* optic lobes [12]. However, how SOL calpain is activated and the identity of its substrates remains unknown. While calcium can activate classical calpains by binding to their unique penta-EF hand domain and their catalytic domain [13] and can also activate atypical calpains such as Tra by binding to the catalytic domain [14], it was shown to have no detectable effect on SOL calpain activity [2]. This is most probably due to the lack of conservation of calcium binding residues in the catalytic domain of SOL calpain [2]. In addition, while the SOL calpain zinc finger domain binds to polyubiquitin, polyubiquitin alone or together with calcium did not activate SOL calpain [2].

In *Aplysia*, expression of a dominant negative catalytically inactivated SOL calpain specifically prevented a form of non-associative long-term facilitation [15]. This may be due to a role of this calpain in cleaving PKCs into persistently active PKMs, since unlike vertebrates, invertebrates lack an alternative transcript that expresses PKM [16]. However, studies using inhibitors and dominant negatives have shown that PKMs still play a role in maintaining memory in this system [15, 17]. As non-associative plasticity in *Aplysia* has not been characterized previously in vertebrates, it is of some interest to determine which neurons express Capn15 to identify candidates for where such non-associative plasticity may occur.

We have recently generated *Capn15* (vertebrate SOL calpain) knockout (KO) mice and showed that loss of *Capn15* leads to a lower Mendelian ratio, a smaller weight of weaned *Capn15* KO mice and developmental eye anomalies (submitted). We have also identified likely pathogenic variants of *CAPN15* in three human individuals with

developmental eye anomalies (submitted), suggesting a conserved role in eye development. Here, using 7 T pre-clinical MR imaging, we reveal a decrease in whole brain volume of adult *Capn15* KO mice, as well as in specific regions, such as the thalamus and certain hippocampal subregions. We further characterize the distribution of Capn15 in the brain of adult *Capn15* KO mice and show that Capn15 remains expressed in the adult hippocampal CA1 neurons and in Purkinje cells in the cerebellum, neurons particularly implicated in synaptic plasticity. We generate a *Capn15* conditional KO mouse (cKO) in which Capn15 is only expressed in a subset of excitatory neurons in the forebrain after early brain development. Unlike *Capn15* KO mice, *Capn15* cKO mice have normal weight, eyes, and brain size.

## Material and methods

### *Capn15* antibody

Polyclonal antibodies were raised in rabbits against the carboxy terminal of Capn15 using the following epitope: CDVAGLHGPRPL. A cysteine residue was added to the N-terminal of the peptide to enhance coupling. Peptides were coupled to KLH-maleimide and SulfoLink coupling resin (Thermo scientific) according to manufacturer's instruction. After conjugation to KLH-maleimide, rabbits were injected and after four boosts the final serum was affinity purified on SulfoLink columns as previously described[18].

### Generation of the *Capn15* conditional KO mouse

Embryonic stem cells with a cassette inserted into the mouse *Capn15* locus (intron 2) were obtained from the International Mouse Phenotyping Consortium (IMPC). The strategy used by the consortium was to insert a cassette that provides a strong exon entry site coupled with a stop codon with lacZ produced from internal ribosome entry site translation [19-20]. To remove the lacZ-Neo cassette, these mice were bred with mice that contain flippase (FLP) recombinase that recognizes a pair of Flp recombinase target (FRT) sequences that flank the genomic region containing this cassette leaving lox sites surrounding the catalytic exons 3-5. These mice were bred against mice expressing germline Cre recombinase to remove the floxed exons and generate a KO line. To generate a conditional KO line, the mice were bred with the CaMKIIα-Cre-CRE T29-1 [21] that only knocks out *Capn15* after development in forebrain excitatory neurons.

**Dissections**

Adult mice were transcardially perfused with ice-cold phosphate-buffered saline (PBS) followed by 4% (wt/vol) ice-cold paraformaldehyde (PFA) in PBS. Brains were post-fixed in 4%PFA for 45min at 4$^{o}$C, rinsed in PBS, and cryoprotected in 30% sucrose/PBS overnight at 4$^{o}$C. The following day, brains were embedded in Tissue-Plus$^{TM}$ O.C.T. compound (Fisher Healthcare) and flash frozen in 2-methylbutane chilled in dry ice. The brains were kept at −80°C until further use. For amygdala dissection, mouse brains were removed and frozen on dry ice and kept at −80°C until further use. The amygdala was dissected from each frozen brain in the cryostat using a neuro punch (0.5 mm; Fine Science Tools). For MRI analysis, adult mice were transcardially perfused with ice-cold PBS followed by 4% (wt/vol) ice-cold PFA in

PBS. Brains were then post-fixed in 4% PFA overnight at 4°C, rinsed in 1XPBS, and stored in 1XPBS + 0.05% sodium azide.

**X-gal staining**

Sections of 20μm were incubated overnight at 37°C in solution containing 80 mM $Na_2HPO_4$, 20 mM $NaH_2PO_4$, 2 mM $MgSO_4$, 5 mM $K_3[Fe(CN)_6]$ , 5 mM $K_4[Fe(CN)_6]$, 0.2% NP-40, 0.1% sodium deoxycholate, and 1.5 mg/ml X-gal. Sections were rinsed in PBS, washed in ethanol (50% for 1min, 70% for 1min, 95% for 1min and 100% for 2X1min), cleared in xylene, and mounted with Permount (Fisher Scientific).

**Immunohistochemistry**

Adult mouse brains were fixed with 2% PLP solution (PBS containing 2% PFA, 10mM sodium periodate, and 70mM L-lysine) for 3 h at 4°C and P3 mouse brains were fixed with 2% PLP solution for 1 hr at 4°C. Brains were cryoprotected in 30% (wt/vol) sucrose in PBS and embedded in OCT (Fisher Healthcare). Brains were frozen on dry ice and cryosectioned (14-μm-thick coronal sections). Sections were first incubated with blocking solution containing 5% (vol/vol) goat serum (or donkey serum for goat antibodies), 0.1% (vol/vol) Triton-X, and 0.5mg/ml BSA in PBS for 1.5 h. Hippocampal and cerebellar sections were incubated with a rabbit polyclonal antibody directed against Purkinje cell protein 4 (PCP4; Sigma, dilution1:400) and a chicken polyclonal antibody directed against β-galactosidase (β-gal; abcam, dilution 1:1000) in the blocking solution overnight at 4°C. After rinsing five times with the blocking solution for 5 min, sections were incubated with a goat anti-chicken IgY secondary antibody conjugated to Alexa

Fluor 594 (Invitrogen, dilution 1:500) and a goat anti-rabbit IgG secondary antibody conjugated to Alexa Fluor 488 (Invitrogen, dilution 1:500) in the blocking solution for 1 h at room temperature. Eye sections were incubated with a chicken polyclonal antibody directed against β-galactosidase (β-gal; abcam, dilution 1:1000) and either a goat polyclonal antibody directed against Brn3a (Santa Cruz, dilution 1:500) or a goat polyclonal antibody directed against ChAT (Millipore Sigma, dilution 1:100) in the blocking solution overnight at 4°C. After rinsing five times with the blocking solution for 5 min, sections were incubated with a goat anti-chicken secondary antibody conjugated to Alexa Fluor 594 (Invitrogen, dilution 1:500) and a donkey anti-goat IgG secondary antibody conjugated to Alexa Fluor 488 (invitrogen, dilution 1:500) in the blocking solution for 1 h at room temperature. DNA was labeled with Hoechst (1:2000) for 3 min and the sections were mounted using fluorescence mounting media (Dako, S3023). All images were taken using a Zeiss Observer Z1 fluorescent microscope using a 10X objective.

**Quantification of Purkinje cell number**

The number of cells in PCP4-labeled Cerebellar sections were counted manually in 8-10 sections through the cerebellum and the density of cells calculated for WT and Capn 15 KO animals by an observer blind to the genetic status of the animal. The average density of the five WT animals was standardized to 1 and the ratio (density of KO animal/average) was calculated and a one sample t-test was used to determine statistical significance.

**Western blotting**

Brains were homogenized manually in lysis buffer containing 25 mM Tris-HCl (pH 7.4), 150 mM NaCl, 6 mM $MgCl_2$, 2 mM EDTA, 1.25% NP-40, 0.125% SDS, 25 mM NaF, 2 mM $Na_4P_2O_7$, 1 mM dithiothreitol (DTT), 1 mM phenylmethylsulfonyl fluoride (PMSF), 20 mg/ml leupeptin, and 4 mg/ml aprotinin. Before loading, 5X sample buffer was added to the lysate and samples were incubated at 95$^{o}$C for 5min. Proteins were resolved by SDS-PAGE on Bis-Tris gel and transferred to nitrocellulose membrane (Bio-Rad). The blots were blocked in TBST (TBS + 0.1% Tween) containing 4% skim milk for 30min at room temperature and then incubated with primary antibodies overnight at 4$^{o}$C. After washing 3 times with TBST, the blots were incubated with HRP-conjugated secondary antibodies for 1 hour at RT, and washed again 3 times in TBST. The Western Lightning Plus-ECL kit (NEL103001EA; PerkinElmer LLC Waltham, MA USA) was used as per manufacturer's instructions to detect protein bands. The primary antibody used was homemade rabbit anti-Capn15 antibody (1:1000) raised against the C-terminus of Capn15. The secondary antibody was horseradish peroxidase-conjugated goat anti-rabbit secondary antibody (1:5000). Antibodies were diluted in Tris buffered saline with Tween containing 4% skim milk powder.

**Eye phenotype quantification**

Mice eyes were examined and grouped as follows: seems normal, obvious cataract, small eye and no eye. This categorisation was performed for both eyes of each mouse. The analysis was performed blind in regards to the genotype of the mice.

**Quantification of immunoblotting** Immunoblots were scanned and imaged using the public domain Image J program developed at the U.S. National Institute of Health (https://imagej.nih.gov/ij/). We calibrated our data with the uncalibrated optical density feature of NIH image, which transforms the data using the formula $\log_{10}[\frac{225}{225-x}]$, where x is the pixel value (0–254). We find that with this correction and including the entire band (which expands near saturation) values are linear with respect to amount of protein over a wide range of values [22]. To be able to use different blots, we used the Ponceau image for each gel to normalize the amount of SOL calpain in brains at different ages to the amount of SOL calpain in E12-E14 brains run on the same gel.

**Image Acquisition** Magnetic resonance imaging was performed using the 7 T Bruker Pharmascan (Bruker Biosciences, Billerica, MA) ultra-high field MRI system of the McConnell Brain Imaging Centre. For imaging, brains were housed in a cylindrical container and immersed in an MR-invisible fluorinated solution, FC-40 (Sigma Aldrich, St. Louis, Missouri), to remove the background MRI signal. For MRI radiofrequency excitation and reception, a 2.3 cm inner diameter volume resonator was utilized. The imaging protocol included a sagittal orientation, 3D steady-state free precession MRI sequence with an echo time (TE) of 5 milliseconds, repetition time (TR) of 10 milliseconds, receiver bandwidth of 50 kHz and excitation pulse flip angle of 30 degrees. The image acquisition matrix was selected to achieve an isotropic voxel resolution of 100 $\mu m^3$. The specific sagittal orientation imaging field of view was $2.3 \times 1.7 \times 1.7$ $cm^3$. 31 signal averages were collected to improve image signal-to-noise ratio, leading to a total scan time of approximately six hours and 60 seconds for the full MRI histology scan. For

image reconstruction, a trapezoidal filter was applied to the complex image data along the first phase encode direction to reduce subtle effects of Gibbs ringing.

**Image Processing and Statistical Analysis** We employed an image registration-based method to investigate anatomical brain volume differences between WT, conditional knockout (cKO) and full knockout (KO) mice. Specifically, an automated, image intensity-based, affine registration [23] was used to align all mouse brains to a common coordinate system. During this registration step, it was determined that the KO mouse brains were, on average, 14% smaller than the WT mouse brains. For this reason, as part of the affine registration, a volumetric pre-scaling was applied to globally scale the KO brain images by a factor of 1.14. The pre-scaling used a nearest neighbour approach. To avoid registration bias caused by differences between our studied population and the mouse template [24], a population-specific average was constructed using an algorithm described in Fonov et al [25]. This step yielded an average image of all the samples included in our cohort. A mouse brain atlas [24] containing reference regions of interest (ROIs) for the thalamus, amygdala, parieto-temporal cortex and whole hippocampus was next used to provide suitable ROIs for volumetric measurement. More specifically, a non-linear registration (ANTs [26]) between the atlas space [24] and our population average was conducted to create an anatomical atlas specific to our mouse population. The deformation fields from the non-linear registration were inverted and blurred with a Gaussian smoothing kernel. The Jacobian determinants of the deformation fields were then extracted to yield estimates of local expansion or contraction at both the ROI and voxel level relative to the population average. Since we also had a specific interest in

volumetric changes in KO mice in the hippocampal sub-fields, a mouse hippocampal sub-field atlas [27] was non-linearly registered [26] and warped to the population average to measure volumes of the cornu ammonis 1 (CA1), CA2, CA3, stratum granulosum and dentate gyrus in the mouse brain images.

We next used a linear model in the R software package [28] to measure the main effect of volume differences (i) in individual ROIs in KO and cKO mice compared to WT mice and (ii) at the voxel-level in KO and cKO mice compared to WT mice. All statistical analyses were corrected for multiple comparisons, utilizing the false discovery rate technique [29] with a 5% threshold.

## Results

### *Capn15 expression and distribution in adult Capn15 KO mice*

We have previously described *Capn15* KO mice [30] and taking advantage of the reporter gene *lacZ* which expression is under the control of the *Capn15* promoter, used X-gal staining to characterize distribution of Capn15 in developing brain. Capn15 was mainly enriched in the mantle zone in E12 embryos, in the subventricular zone, immediately next to the ventricular zone and in specific areas of the hippocampus in E18 embryos and was ubiquitously expressed in the brain in P3 mice [30]. Most notably, Capn15 was expressed in the adult brain at remarkably lower levels than in the developing brain but was specifically enriched in the adult hippocampus [30]. To expand on these results, we more fully examined Capn15 distribution in adult *Capn15*$^{(lacZ\text{-}Neo)}$ heterozygous mice using X-gal staining. As shown in Fig.1, Capn15 is still expressed in specific sets of neurons in the mature brain, including the hippocampus, amygdala, and

cortex. A closer look at the hippocampal region shows an unequal distribution of staining. Excitatory pyramidal neurons in CA1 and CA3 and some cells located in stratum radiatum are stained. However, a gap near the expected position of CA2 was seen and in the dentate gyrus, Capn15 is expressed at low levels in the subgranular zone and showed the strongest signal in the molecular layer of dentate gyrus. This region contains mainly interneurons such as molecular layer perforant pathway cells (MOPP) [31] and neurogliaform cells [32] as well as astrocytes [33].To confirm the result obtained with X-gal staining, we stained sections from adult WT and *Capn15* KO mice brains with our Capn15 antibody. Unfortunately, this antibody lacked specificity in immunohistochemistry and could not be used to this end. Thus, we took advantage of the *lacZ* reporter and stained sections from adult *Capn15-lacZ* mice with an anti β-galactosidase (β-gal) antibody as well as an antibody directed a CA2 marker (PCP4; [34]) to confirm the lack of Capn15 in CA2 (Fig.2). DNA was labeled with Hoechst. The anti-β-galactosidase (β-gal) antibody appeared as punctated spots (Fig.2), perhaps due to aggregation or specific localization of the enzyme in neurons. To confirm β-gal antibody specificity, we co-stained sections from WT mouse brain with the anti β-gal antibody and Hoechst. As shown in Fig.2, a weak diffuse signal was observed in WT mice indicating specificity of the punctated staining in *Capn15-lacZ* mice and our result confirms the absence of Capn15 from CA2 (Fig.2). When examining the staining with the β-gal antibody, we noted a striking difference between the punctated spots in the pyramidal neurons and in the molecular layer. This was most obvious comparing staining in CA3 neurons and the molecular layer in the same sections, where the majority of X-gal reactivity in the hippocampus was located (Fig. 3). The punctated spots in the molecular

layer appeared smaller, more numerous and less associated with nuclei (as seen by Hoechst staining; Fig. 3). While not definitive, it is possible that this represents Capn15 expression in astrocytes.

Staining in the Purkinje neurons was confirmed with stained sections from adult *Capn15-lacZ* mice with the anti-β-gal antibody as well as PCP4, which was originally described as a Purkinje cell marker [35]. DNA was labeled with Hoechst. As shown in Fig.4, Capn15 was enriched in Purkinje cells in the cerebellum. As loss of *Capn15* was linked to neurodgeneration in *Drosophila*, we determined whether the loss of *Capn15* led to a loss of Purkinje cell neurons. *Capn15* KO animals had the same number of Purkinje cells as WT littermates (1.01 ± 0.25 normalized to WT; $n$=5; SD, $p$>0.5, one sample t-test).

As homozygous disruption of *Capn15* leads to abnormal eye development, we examined Capn15 staining in the eye, although in this case we focused on an earlier stage of development, P3. At this stage, X-gal staining is mainly restricted to the retinal ganglion cell layer. To confirm expression of Capn15 in retinal ganglion cells, we examined co-localization of β-gal with a marker for retinal ganglion cells, Brn3a (Fig.5; [36]. As shown in Fig.5, the two markers co-localized (79 ± 5 of ; β-gal cells colocalized with Brn3a, $n$=2) but only about half of the retinal ganglion cells contained β-gal (44 ± 2 Brn3a neurons co-localized with β-gal). We also examined co-localization of β-gal with ChAT as a fraction of retinal ganglion cells that do not contain Brn3a are displaced cholinergic amacrine cells [37]. Similar to Brn3a staining, about half of the ChAT labelled neurons co-localized with β-gal (62 ± 5, n=2). Thus, Capn15 is expressed mainly in the retinal ganglion cell layer in a subset of Brn3a+ and ChAT+ cells.

***Capn15 conditional KO mice have normal weight and no eye deficits***

We have previously shown that the homozygous loss of *Capn15* decreases embryonic survival and weaned mice weigh less than their WT and heterozygous littermates [30]. Furthermore, *Capn15* KO mice had mild to severe eye deficits that ranged from cataracts to microphthalmia (small eye) and anophthalmia (no eye). These eye anomalies were also present in younger animals suggesting they were not due to a degenerative process [30].To further test this, we generated *Capn15* conditional KOs (cKOs) as described in Methods and a CaMKIIα-Cre line was used to this end. CaMKIIα-Cre transgenic mice have the mouse calcium/calmodulin-dependent protein kinase II alpha promoter driving Cre recombinase expression in a subset of excitatory neurons in the forebrain including the hippocampus and the amygdala and CRE is not expressed until after P14 [38]. As shown in Figs.6A and 6B, Capn15 protein levels are significantly decreased in homogenates from *Capn15* cKO adult mice amygdala indicating successful disruption of the *Capn15* gene in cKO mice (**$p$=0.002, Student's t-test; n=4 cKO, 3 WT). In contrast, there was little decrease seen in the hippocampus (Figs. 6C and 6D), confirming that most of Capn15 expression (molecular layer of dentate gyrus), is not in excitatory neurons in this structure. Furthermore, a thorough assessment of these mice showed no weight difference compared to WT mice ($p$=0.16, Student's t-test; n=26 for the WT group composed of *Capn15* cKO Cre- littermates and n=15 for the *Capn15* cKO group; Fig.6E) and most importantly no eye deficits (Fig.6F, n=20 *Capn15* cKO, WT).

***MRI analysis of Capn15 KO and Capn15 cKO adult brains***

In *Drosophila*, loss of the SOL calpain was mainly reported to cause deficits in the optic lobe. However, it is not clear how extensively this has been analyzed. To use a non-biased screen to determine which brain regions are affected by the loss of *Capn15*, we used whole brain MRI on 14 WT (9 M, 5F), 8 *Capn15* KO (4M, 4F) animals and 5 *Capn15* cKO (5 male). There was no difference in whole brain volume between male and female mice for either the WT (p=0.97) or the *Capn15* KO groups (p=0.83). Accordingly, males and females were grouped together for statistical analysis. There was a highly significant, 14% decrease in whole brain volume in the *Capn15* KO animals (p=7.32e-7) compared to the WT animals. We further noted a significant decrease in the hemisphere-averaged volume of the thalamus in *Capn15* KO animals compared to the corresponding WT animals (p=1.28e-5; Figs.7A and 7C) after compensating for the overall decrease in brain size (See Methods). There was no difference in thalamic volume between *Capn15* cKO and WT animals (p=0.35; Figs.7A and 7C). Atlas-based region of interest analysis revealed an increase in the amygdala volume of *Capn15* KO mice compared to WT mice (p=0.003, Figs.7A and 7C). However, there was no corresponding difference between *Capn15* cKO and WT mice (p=0.42). As well, there were no differences in volume of the parieto-temporal cortex between either *Capn15* KO or cKO mice and corresponding WT mice (Figs.7A and 7C). We also used voxel-based morphometry to measure local differences in volume between *Capn15* KO and WT mice. Twelve representative slices having locally decreased volume of *Capn15* KO brain compared to WT brain (blue colours) and the corresponding locally increased volume (yellow/orange colours) are

presented in Fig.7B. Volume decreases in *Capn15* KO mouse brain are notable (light blue colours) in the hippocampus, superior parietal cortex and thalamus.

Additional attention in our high resolution, MRI-based volume analysis was given to the hippocampus due to the possible role of Capn15 in synaptic plasticity [15, 39]. An image of the hippocampal sub-field atlas we employed for sub-field volumetry is shown in Fig. 8A. We did not observe differences in overall hippocampal volume between either *Capn15* KO or *Capn15* cKO mice and the corresponding WT animals. However, voxel-level differences in hippocampal volume were observed between *Capn15* KO and WT mice when we restricted our linear model statistical analysis to regions inside the hippocampal sub-fields (Figs.8A and 8C). In particular, there were voxel decreases in hippocampal volume for mid-line slices of the *Capn15* KO mice brain compared to the WT mice. Examination of the hippocampal sub-fields using region of interest-based analysis identified decreases in the CA1 ($p=0.001$), the CA2 ($p=0.002$), the dentate gyrus ($p=0.05$) and the stratum granulosum ($p=0.03$) volume of *Capn15* KO mice when compared to WT mice (Figs.8A and 8C). Notably, such volumetric differences were not observed in CA3. However, it is possible that significant changes in volume are taking place in sub-regions of the CA3 area but the atlas label includes both regions that increase and regions that decrease in volume which may explain why the box plot does not show statistically significant aggregate volume change in the CA3 label. As well, no differences in hippocampal sub-field volume were observed between *Capn15* cKO and WT mice. We further performed a voxel-level statistical analysis of contraction/expansion inside the hippocampus. As shown in Fig.8B, volume decreases in

*Capn15* KO mouse brain are notable (light blue colours) in the CA1, CA2, dentate gyrus and stratum granulosum whereas increases (orange) are noted in the CA3 area.

**Discussion**

We have previously described *Capn15* KO mice and found that they had a lower body weight and striking ocular anomalies when compared to their WT littermates. In this paper, we further characterize these mice using localization of Capn15 expression and MR imaging and show that Capn15 is expressed in a variety of brain regions in the adult and that the loss of Capn15 leads to smaller brains and specific changes in the thalamus, amygdala and hippocampal subfields.

The average weight of a whole *Capn15* KO mouse is 10% smaller compared to its WT littermate [30]. MRI results showed that the *Capn15* KO brain is also 14% smaller in volume compared to the WT animals. This brings up the possibility that the total 14% change in brain volume could be due to the proportional 10% weight loss, although there is no clear evidence in the literature that a decrease in overall weight leads to a decrease in brain volume. The brain makes up only a small fraction of the weight of the mouse, so the decrease in brain volume cannot explain the overall weight difference.

Certain brain areas such as subfields of the hippocampus and thalamus are still significantly smaller taking the 14% global change into account, inconsistent with a general decrease in brain size due to the lower weight of the *Capn15* KO mice. On the other hand, the amygdala is significantly larger in *Capn15* KO mice after scaling, indicating that this region is relatively spared. Unlike *Drosophila*, the loss of *Capn15* leads to a less severe neurodevelopmental phenotype, although it should be noted that

only viable *Capn15* KOs were examined and based on Mendelian ratios, only 50% of *Capn15* KO animals survive to weaning, thus it is possible that the mice that did not survive to weaning had more severe neuronal losses.

There does not appear to be a relationship between where Capn15 is expressed in the mature brain and the regions mostly affected by *Capn15* loss during development. For example, Purkinje neurons highly express *Capn15*, but the cerebellum is not an area that is specifically affected as observed in MRI and the number of Purkinje neurons was not affected in *Capn15* KO mice. In contrast, CA2 neurons do not express *Capn*15 in the adult, but brain MRI suggests that CA2 area is decreased in size in the *Capn15* KO animals. The lack of any changes in the *Capn15* cKO mouse in brain size and eye phenotypes, coupled with the wide and increased expression of Capn15 early in brain development, suggest that most of the phenotypes (brain size, eye development) we have examined occur due to an early developmental role of Capn15. The continued expression of Capn15 in brain areas involved in plasticity are consistent with a possible later role in plasticity, as has been seen in *Aplysia* [15].

The expression pattern of Capn15 seems quite varied. In the area examined most closely, the hippocampus, it is expressed in CA1 and CA3 excitatory neurons, but not in CA2 or granule neurons. The largest expression may be in the dentate gyrus molecular neuron, perhaps in astrocytes, but such diffuse staining was not seen in other brain regions, such as the cortex or amygdala. Indeed, based on results in the *Capn15* cKO mice, virtually all reactivity in the amygdala was in excitatory neurons as, based on immunoblots, almost all protein was removed in the amygdala in *Capn15* cKO mice. We

have examined single cell databases of neurons, but in general Capn15 is expressed at low levels and is only unreliably detected in most databases.

**Acknowledgments**

This work was supported by CIHR grant MOP 340328 to WSS. The authors would like to thank Mireille Bouchard-Levasseur for excellent technical assistance in quantification of the transgenic mice eye phenotype and Dr. Len Levine for advice concerning the eye phenotype

**Figure legends**

**Figure 1. Capn15 distribution in *Capn15*$^{(lacZ\text{-}Neo)}$ heterozygous mice brain.** X-gal staining of coronal sections from adult *Capn15*$^{(lacZ\text{-}Neo)}$ heterozygous mice hippocampus, amygdala, cortex and cerebellum and from P3 eyes are shown. Scale bar is 100µm except for the P3 eye where the scale bar is 200 µm. LA, lateral amygdale; BLA, basal lateral amygdala; RGC, retinal ganglion cells; GL, granular layer; ML, molecular layer.

**Figure 2. *Capn15* distribution in the hippocampus. A)** The distribution of a CA2 marker (PCP4) and that of β-galacatosidase (β-gal) is shown in sections from adult *Capn15-lacZ* brains. The rabbit polyclonal anti-PCP4 and the chicken polyclonal anti-β-gal antibodies were revealed by using a secondary anti-rabbit conjugated to Alexa Fluor 488 and a secondary anti-chicken conjugated to Alexa Fluor 594 respectively. DNA was labeled with Hoechst. Capn15 seems to be enriched in all hippocampal areas except in CA2 (inset). **B)** The distribution of β-galacatosidase (β-gal) is shown in hippocampal sections from adult *Capn15-lacZ* brains. The chicken polyclonal anti-β-gal antibody were revealed by using a secondary anti-rabbit conjugated to Alexa Fluor 488. DNA was labeled with Hoechst. Capn15 appears to have a distinct expression pattern in the CA3 area and the molecular layer of the hippocampus. GL, granular layer; ML, molecular layer.

**Figure 3. *Capn15* distribution in the cerebellum and eye. A)** The distribution of a Purkinje cell marker (PCP4) and β-galacatosidase (β-gal) is shown in sections from adult *Capn15-lacZ* brains. The rabbit polyclonal anti-PCP4 and the chicken polyclonal anti-β-

gal antibodies were revealed by using a secondary anti-rabbit conjugated to Alexa Fluor 488 and a secondary anti-chicken conjugated to Alexa Fluor 594 respectively. DNA was labeled with Hoechst. Capn15 seems to be enriched in Purkinje cells in the cerebellum. B) The distribution of a retinal ganglion cell marker (Brn3a) or that of cholinergic amacrine cell marker (ChAT) is shown along with that of β-galacatosidase (β-gal) in sections from adult *Capn15-lacZ* brains. The chicken polyclonal antibody directed against β-gal and either the goat polyclonal antibody directed against Brn3a or the goat polyclonal antibody directed against ChAT were revealed by using a goat anti-chicken secondary antibody conjugated to Alexa Fluor 594 and a donkey anti-goat IgG secondary antibody conjugated to Alexa Fluor 488. Capn15 seems to be expressed in the retinal ganglion cell layer in a subset of Brn3a+ and ChAT+ cells.

**Figure 4. *Capn15* cKO mice have normal eyes.** Amygdala **(A)** and hippocampus **(C)** were dissected and homogenized and SDS-PAGE and western blotting were performed as described in Methods. **(B)** Quantification of *Capn15* expression in WT and *Capn15* cKO amygdala shows that Capn15 protein levels are significantly decreased in *Capn15* cKO adult mice amygdala. **(D)** Quantification of *Capn15* expression in WT and *Capn15* cKO hippocampi shows that Capn15 protein levels are not significantly decreased in *Capn15* cKO adult mice hippocampus. **(E)** Animals were weighed after weaning. Average weight of *Capn15* cKO was normalized to average weight of the WT mice. Error bars represent SEM. **(F)** Percentage of mice having eye deficits is compared between WT and *Capn15* cKO mice. Mice were grouped in 4 categories: Seems normal,

obvious cataract, small eye and no eye and this scoring was performed on both left and right eye for each mouse. All of *Capn15* cKO mice eyes seemed normal.

**Figure 5. Whole-brain visualization of significant decreases in brain structure volume in *Capn15* KO and cKO mice relative to WT mice. (A)** The top two rows correspond to 20 axial sections through the mouse brain, the middle two rows correspond to 20 sagittal sections through the brain and the bottom two rows correspond to 20 coronal sections. Each section has a thickness of 100 micrometers. Blue/purple colours identify local voxel-level brain structure volume decrease calculated with a general linear model using false discovery rate correction with a q-threshold of 0.05. **(B)** Magnified coronal views through the mouse mid-brain displaying regional volume decrease (blue colours) and increase (orange) for *Capn15* KO mice compared to WT mice. Each slice through the mid-brain has a thickness of 100 micrometers. The specific position of each slice along the anterior-posterior axis of the mouse brain is shown, overlaid on a sagittal brain slice, in the top right hand corner of the figure. The colours represent t-statistical values calculated with a general linear model using a false discovery rate correction with a q-threshold of 0.05. **(C)** Box and whisker plots showing structure-specific brain volume differences between WT, KO and conditional knockout (cKO) mice. The left-most box and whisker plot labeled 'Scale' corresponds to measurements of whole-brain volume normalized to the atlas mouse brain.

**Figure 6. Hippocampal subfield-specific volume changes in *Capn15* KO and cKO mice compared to WT mice. (A)** A hippocampal sub-field atlas [27] was applied to

evaluate volumetric changes in the hippocampal subfields. The sub-field atlas includes region of interest labels demarcating the dentate gyrus (red), stratum granulosum (blue), CA1 (green), CA2 (purple) and CA3 (orange). **(B)** Voxel-level statistical analysis of contraction/expansion inside the hippocampus. Magnified coronal views through the mouse mid-brain display regional volume decrease (blue colours) and increase (orange) for *Capn15* KO mice compared to WT mice. Each slice through the mid-brain has a thickness of 100 micrometers. The specific position of each slice along the anterior-posterior axis of the mouse brain is shown, overlaid on a sagittal brain slice, in the top right hand corner of the figure. The colours represent t-statistical values calculated with a general linear model using a false discovery rate correction with a q-threshold of 0.05. **(C)** Box and whisker plots showing hippocampal subfield-specific volume differences between WT, KO and cKO mice.

## References


1. Guroff G (1964) A Neutral, Calcium-Activated Proteinase from the Soluble Fraction of Rat Brain. The Journal of biological chemistry 239:149-155.
2. Hastings MH, Qiu A, Zha C, et al. (2018) The zinc fingers of the small optic lobes calpain bind polyubiquitin. Journal of neurochemistry 146:429-445.
3. Zhao S, Liang Z, Demko V, et al. (2012) Massive expansion of the calpain gene family in unicellular eukaryotes. BMC evolutionary biology 12:193.
4. Hastings MH, Gong K, Freibauer A, Courchesne C, Fan X, Sossin WS (2017) Novel calpain families and novel mechanisms for calpain regulation in Aplysia. PloS one 12:e0186646.
5. Shimizu K, Phan T, Mansuy IM, Storm DR (2007) Proteolytic degradation of SCOP in the hippocampus contributes to activation of MAP kinase and memory. Cell 128:1219-1229.
6. Khoutorsky A, Yanagiya A, Gkogkas CG, et al. (2013) Control of synaptic plasticity and memory via suppression of poly(A)-binding protein. Neuron 78:298-311.
7. Briz V, Baudry M (2017) Calpains: Master Regulators of Synaptic Plasticity. The Neuroscientist : a review journal bringing neurobiology, neurology and psychiatry 23:221-231.
8. Liu Y, Wang Y, Zhu G, Sun J, Bi X, Baudry M (2016) A calpain-2 selective inhibitor enhances learning & memory by prolonging ERK activation. Neuropharmacology 105:471-477.
9. Wang Y, Zhu G, Briz V, Hsu YT, Bi X, Baudry M (2014) A molecular brake controls the magnitude of long-term potentiation. Nat Commun 5:3051.
10. Dutt P, Croall DE, Arthur JS, et al. (2006) m-Calpain is required for preimplantation embryonic development in mice. BMC Dev Biol 6:3.
11. Delaney SJ, Hayward DC, Barleben F, Fischbach KF, Miklos GL (1991) Molecular cloning and analysis of small optic lobes, a structural brain gene of Drosophila melanogaster. Proceedings of the National Academy of Sciences of the United States of America 88:7214-7218.
12. Fischbach KF, Heisenberg M (1981) Structural brain mutant of Drosophila melanogaster with reduced cell number in the medulla cortex and with normal optomotor yaw response. Proceedings of the National Academy of Sciences of the United States of America 78:1105-1109.
13. Moldoveanu T, Hosfield CM, Lim D, Elce JS, Jia Z, Davies PL (2002) A Ca(2+) switch aligns the active site of calpain. Cell 108:649-660.
14. Sokol SB, Kuwabara PE (2000) Proteolysis in Caenorhabditis elegans sex determination: cleavage of TRA-2A by TRA-3. Genes Dev 14:901-906.
15. Hu J, Adler K, Farah CA, Hastings MH, Sossin WS, Schacher S (2017) Cell-Specific PKM Isoforms Contribute to the Maintenance of Different Forms of Persistent Long-Term Synaptic Plasticity. The Journal of neuroscience : the official journal of the Society for Neuroscience 37:2746-2763.
16. Bougie JK, Lim T, Farah CA, et al. (2009) The atypical protein kinase C in Aplysia can form a protein kinase M by cleavage. Journal of neurochemistry 109:1129-1143.
17. Cai D, Pearce K, Chen S, Glanzman DL (2011) Protein kinase M maintains long-term sensitization and long-term facilitation in aplysia. The Journal of neuroscience : the official journal of the Society for Neuroscience 31:6421-6431.
18. Sossin WS (2003) Phosphopeptide-specific antibodies to protein kinase C. Methods Mol Biol 233:233-244.

19. Brown SD, Moore MW (2012) The International Mouse Phenotyping Consortium: past and future perspectives on mouse phenotyping. Mamm Genome 23:632-640.
20. Skarnes WC, Rosen B, West AP, et al. (2011) A conditional knockout resource for the genome-wide study of mouse gene function. Nature 474:337-342.
21. Tsien JZ, Chen DF, Gerber D, et al. (1996) Subregion- and cell type-restricted gene knockout in mouse brain. Cell 87:1317-1326.
22. Nakhost A, Forscher P, Sossin WS (1998) Binding of protein kinase C isoforms to actin in Aplysia. Journal of neurochemistry 71:1221-1231.
23. Collins DL, Neelin P, Peters TM, Evans AC (1994) Automatic 3D intersubject registration of MR volumetric data in standardized Talairach space. J Comput Assist Tomogr 18:192-205.
24. Kovacevic N, Henderson JT, Chan E, et al. (2005) A three-dimensional MRI atlas of the mouse brain with estimates of the average and variability. Cereb Cortex 15:639-645.
25. Fonov V, Evans AC, Botteron K, et al. (2011) Unbiased average age-appropriate atlases for pediatric studies. Neuroimage 54:313-327.
26. Avants BB, Epstein CL, Grossman M, Gee JC (2008) Symmetric diffeomorphic image registration with cross-correlation: evaluating automated labeling of elderly and neurodegenerative brain. Med Image Anal 12:26-41.
27. Badhwar A, Lerch JP, Hamel E, Sled JG (2013) Impaired structural correlates of memory in Alzheimer's disease mice. Neuroimage Clin 3:290-300.
28. Pinheiro J, Bates D (2000) Mixed-Effects Models in S and S-PLUS. Springer.
29. Genovese CR, Lazar NA, Nichols T (2002) Thresholding of statistical maps in functional neuroimaging using the false discovery rate. Neuroimage 15:870-878.
30. Zha C, Farah CA, R. H, et al. (2020) Mouse and human studies support a role for CAPN15 variants in cataract and microphthalmia. Genome Medicine Submitted.
31. Li Y, Stam FJ, Aimone JB, Goulding M, Callaway EM, Gage FH (2013) Molecular layer perforant path-associated cells contribute to feed-forward inhibition in the adult dentate gyrus. Proceedings of the National Academy of Sciences of the United States of America 110:9106-9111.
32. Armstrong C, Szabadics J, Tamas G, Soltesz I (2011) Neurogliaform cells in the molecular layer of the dentate gyrus as feed-forward gamma-aminobutyric acidergic modulators of entorhinal-hippocampal interplay. J Comp Neurol 519:1476-1491.
33. Pilegaard K, Ladefoged O (1996) Total number of astrocytes in the molecular layer of the dentate gyrus of rats at different ages. Anal Quant Cytol Histol 18:279-285.
34. Lein ES, Callaway EM, Albright TD, Gage FH (2005) Redefining the boundaries of the hippocampal CA2 subfield in the mouse using gene expression and 3-dimensional reconstruction. J Comp Neurol 485:1-10.
35. Ziai MR, Sangameswaran L, Hempstead JL, Danho W, Morgan JI (1988) An immunochemical analysis of the distribution of a brain-specific polypeptide, PEP-19. Journal of neurochemistry 51:1771-1776.
36. Nadal-Nicolas FM, Jimenez-Lopez M, Sobrado-Calvo P, et al. (2009) Brn3a as a marker of retinal ganglion cells: qualitative and quantitative time course studies in naive and optic nerve-injured retinas. Invest Ophthalmol Vis Sci 50:3860-3868.
37. Jeon CJ, Strettoi E, Masland RH (1998) The major cell populations of the mouse retina. The Journal of neuroscience : the official journal of the Society for Neuroscience 18:8936-8946.
38. Sonner JM, Cascio M, Xing Y, et al. (2005) Alpha 1 subunit-containing GABA type A receptors in forebrain contribute to the effect of inhaled anesthetics on conditioned fear. Molecular pharmacology 68:61-68.

39. Hu J, Ferguson L, Adler K, et al. (2017) Selective Erasure of Distinct Forms of Long-Term Synaptic Plasticity Underlying Different Forms of Memory in the Same Postsynaptic Neuron. Current biology : CB 27:1888-1899 e1884.

# Figure 1

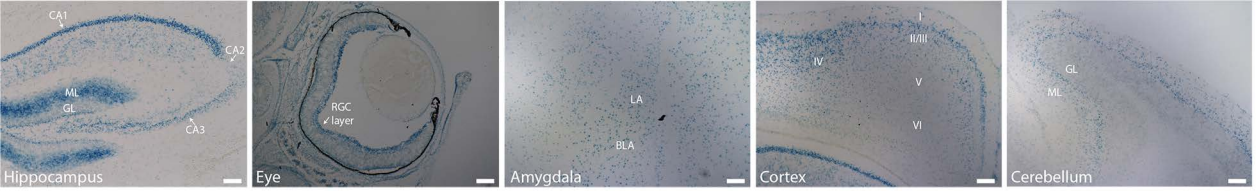
CA1
CA2
ML
GL
CA3
Hippocampus
RGC
layer
Eye
LA
BLA
Amygdala
I
II/III
IV
V
VI
Cortex
GL
ML
Cerebellum

# Figure 2

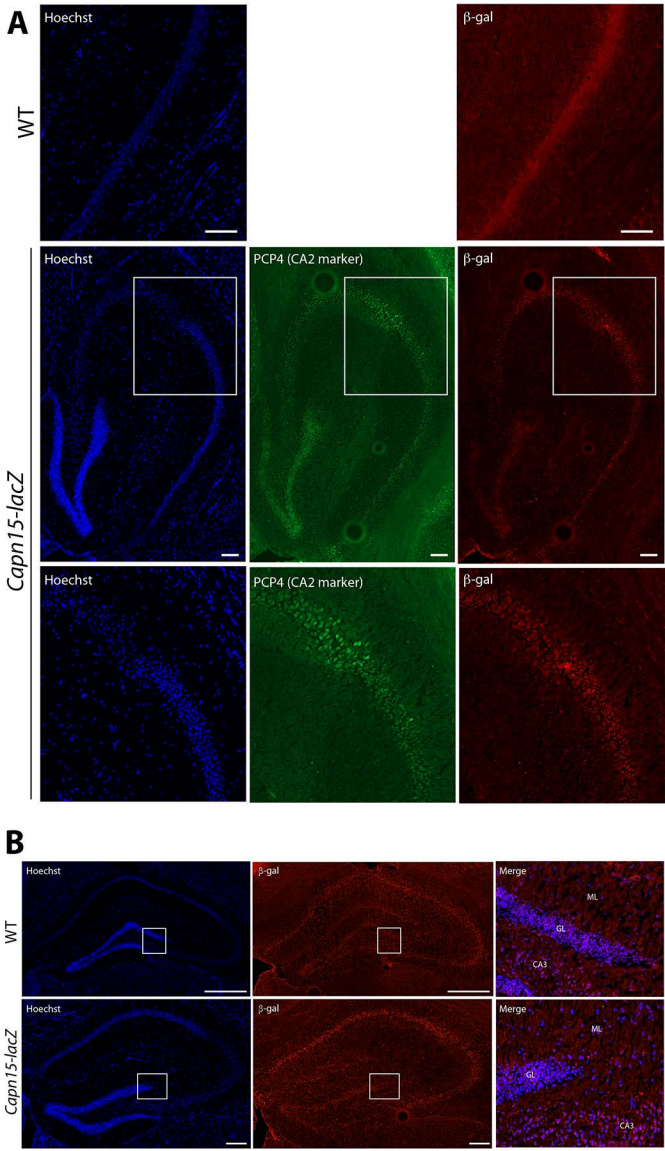
A
WT
Hoechst
β-gal
Capn15-lacZ
Hoechst
PCP4 (CA2 marker)
β-gal
Hoechst
PCP4 (CA2 marker)
β-gal
B
WT
Hoechst
β-gal
Merge
ML
GL
CA3
Capn15-lacZ
Hoechst
β-gal
Merge
ML
GL
CA3

# Figure 3

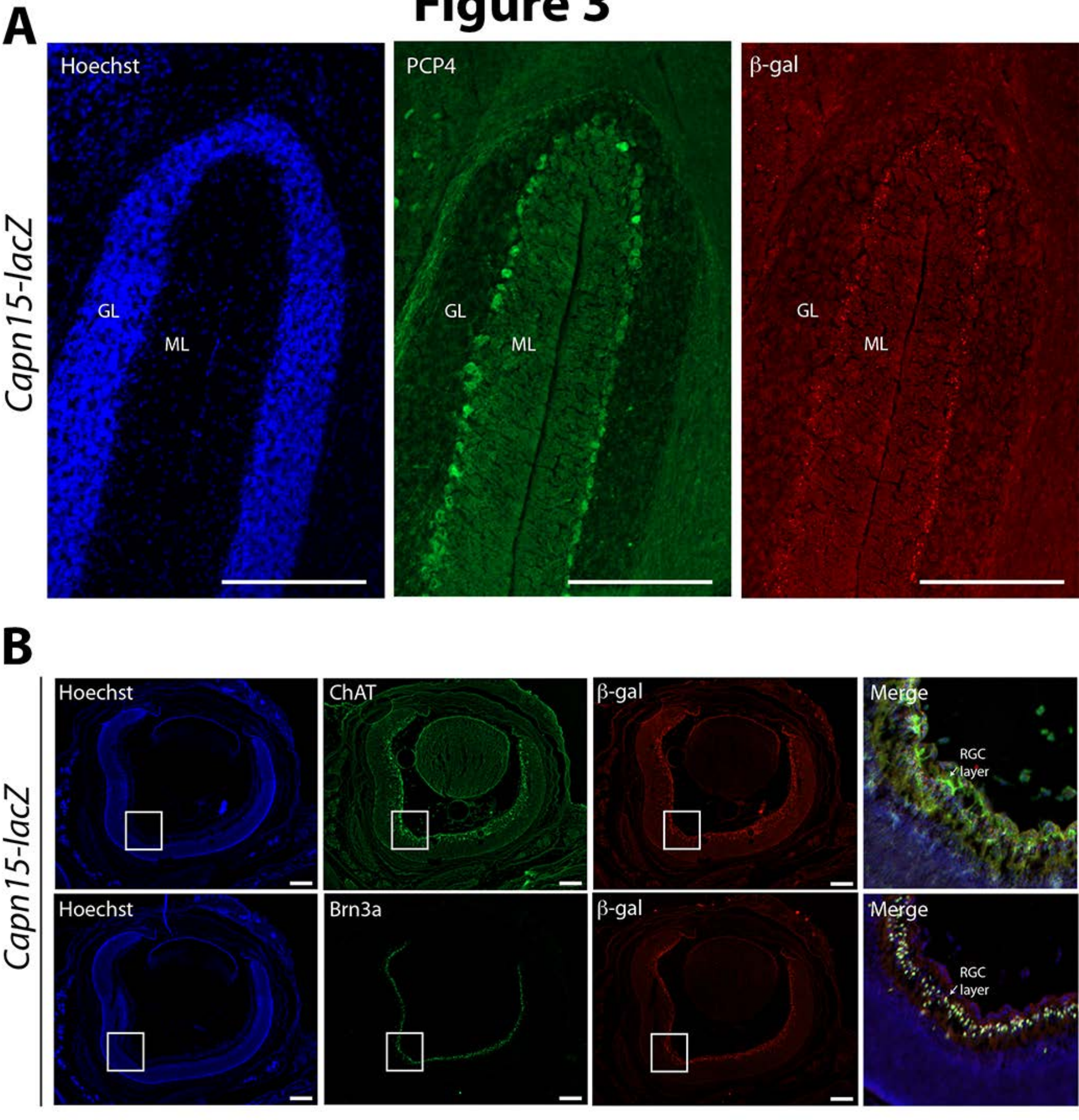
A
Capn15-lacZ
Hoechst
PCP4
β-gal
GL
ML
GL
ML
GL
ML
B
Capn15-lacZ
Hoechst
ChAT
β-gal
Merge
RGC layer
Hoechst
Brn3a
β-gal
Merge
RGC layer

# Figure 4

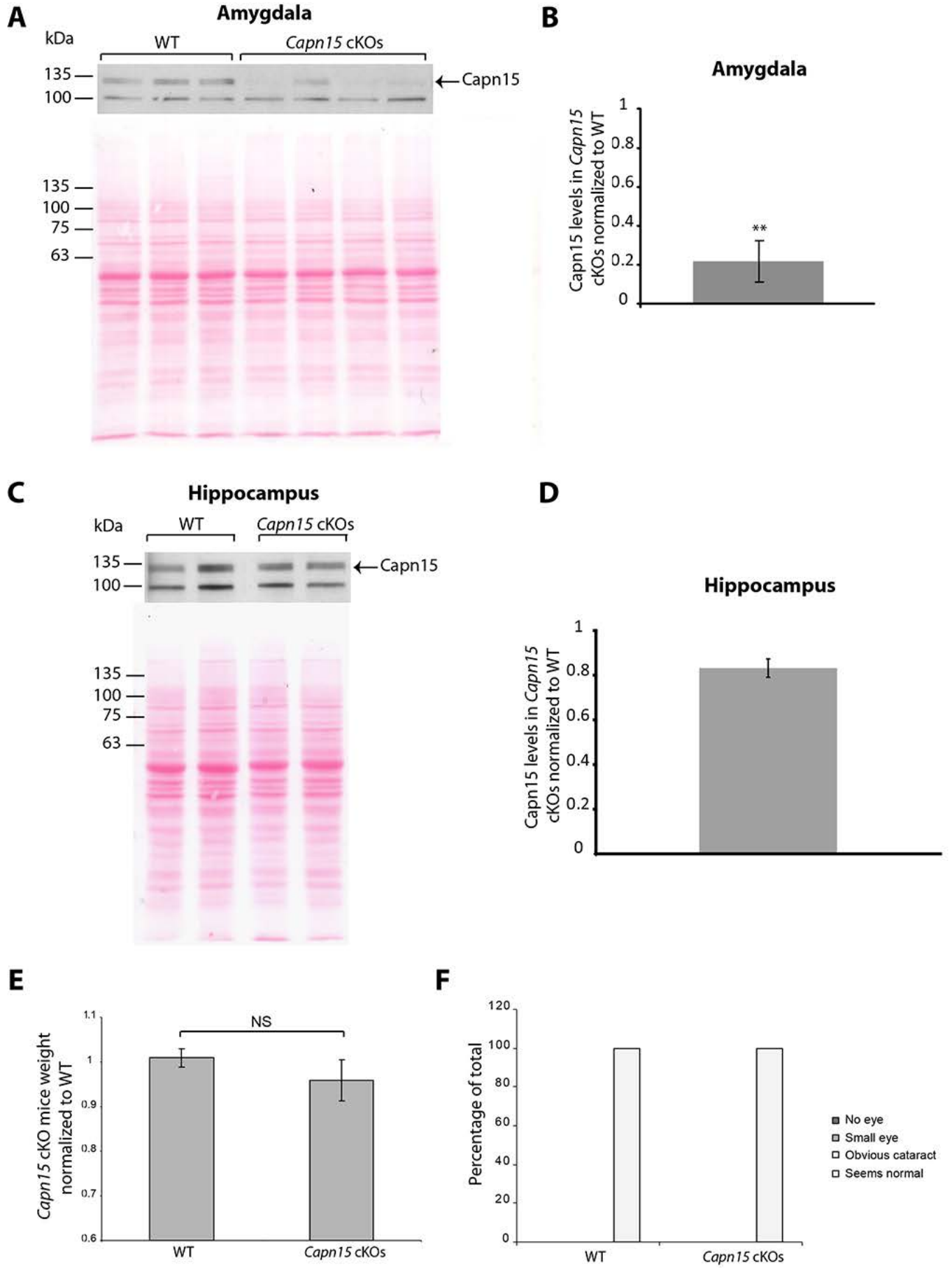
A
Amygdala
kDa
WT
Capn15 cKOs
135
100
Capn15
135
100
75
63
B
Amygdala
Capn15 levels in Capn15 cKOs normalized to WT
1
0.8
0.6
0.4
0.2
0
**
C
Hippocampus
kDa
WT
Capn15 cKOs
135
100
Capn15
135
100
75
63
D
Hippocampus
Capn15 levels in Capn15 cKOs normalized to WT
1
0.8
0.6
0.4
0.2
0
E
Capn15 cKO mice weight normalized to WT
1.1
1
0.9
0.8
0.7
0.6
NS
WT
Capn15 cKOs
F
Percentage of total
120
100
80
60
40
20
0
WT
Capn15 cKOs
No eye
Small eye
Obvious cataract
Seems normal

# Figure 5

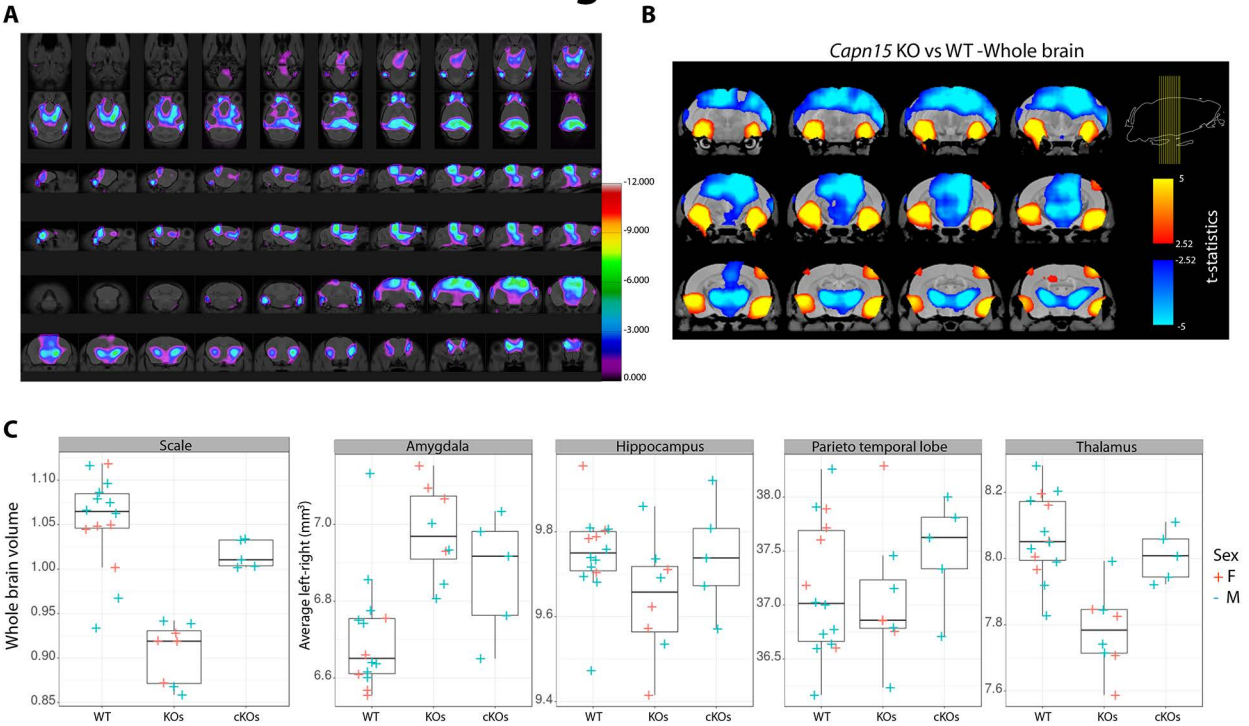
A
-12.000
-9.000
-6.000
-3.000
0.000
B
*Capn15* KO vs WT -Whole brain
5
2.52
-2.52
-5
t-statistics
C
Scale
Whole brain volume
1.10
1.05
1.00
0.95
0.90
0.85
WT
KOs
cKOs
Amygdala
Average left-right (mm³)
7.0
6.8
6.6
Hippocampus
9.8
9.6
9.4
Parieto temporal lobe
38.0
37.5
37.0
36.5
Thalamus
8.2
8.0
7.8
7.6
Sex
F
M

# Figure 6

A

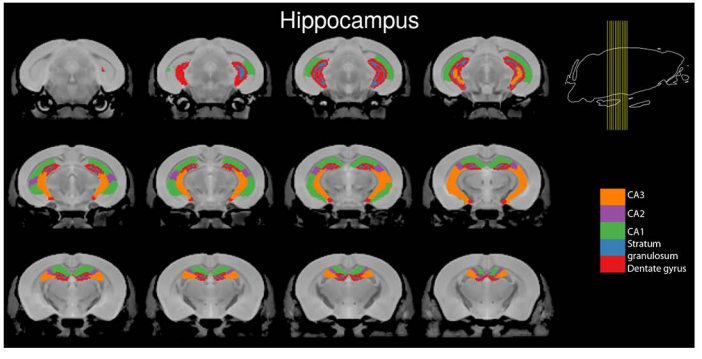
Hippocampus
CA3
CA2
CA1
Stratum granulosum
Dentate gyrus

B

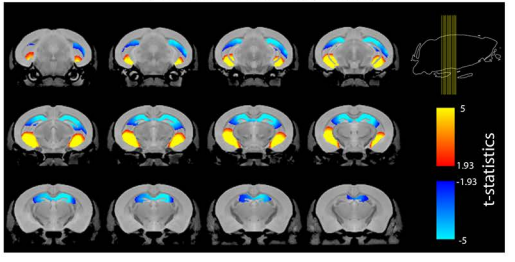
*Capn15* KO vs WT -Hippocampus
5
1.93
-1.93
-5
t-statistics

C

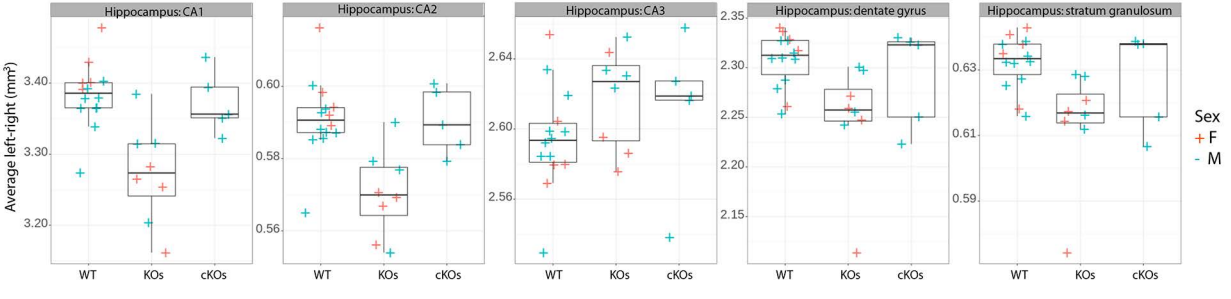
Hippocampus: CA1
Hippocampus: CA2
Hippocampus: CA3
Hippocampus: dentate gyrus
Hippocampus: stratum granulosum
Average left-right (mm³)
3.40
3.30
3.20
0.60
0.58
0.56
2.64
2.60
2.56
2.35
2.30
2.25
2.20
2.15
0.63
0.61
0.59
WT
KOs
cKOs
Sex
F
M